Quantification of large transmural biopsies reveals heterogeneity in innervation patterns in chronic myocardial infarction

Chen, H.S.; Voortman, L.M.; Munsteren, C. van; Wisse, L.J.; Tofig, B.J.; Kristiansen, S.B.; ... ; Jongbloed, M.R.M.

JACC: CLINICAL ELECTROPHYSIOLOGY VOL. 9, NO. 8, 2023

PUBLISHED BY ELSEVIER

ORIGINAL RESEARCH

VENTRICULAR ARRHYTHMIAS - PATHOPHYSIOLOGY

Quantification of Large Transmural Biopsies Reveals Heterogeneity in Innervation Patterns in Chronic Myocardial Infarction

H. Sophia Chen, MD,[a,b] Lenard M. Voortman, PhD,[c] J. Conny van Munsteren, BASc,[b] Lambertus J. Wisse, BASc,[b] Bawer J. Tofig, MD,[d] Steen B. Kristiansen, MD, PhD,[d] Claire A. Glashan, MD,[a,b] Marco C. DeRuiter, PhD,[b] Katja Zeppenfeld, MD, PhD,[a,*] Monique R.M. Jongbloed, MD, PhD[a,b,*]

ABSTRACT

BACKGROUND Abnormal cardiac innervation plays an important role in arrhythmogenicity after myocardial infarction (MI). Data regarding reperfusion models and innervation abnormalities in the medium to long term after MI are sparse. Histologic quantification of the small-sized cardiac nerves is challenging, and transmural analysis has not been performed.

OBJECTIVES This study sought to assess cardiac innervation patterns in transmural biopsy sections in a porcine reperfusion model of MI (MI-R) using a novel method for nerve quantification.

METHODS Transmural biopsy sections from 4 swine (n = 83) at 3 months after MI-R and 3 controls (n = 38) were stained with picrosirius red (fibrosis) and beta-III-tubulin (autonomic nerves). Biopsy sections were classified as infarct core, border zone, or remote zone. Each biopsy section was analyzed with a custom software pipeline, allowing calculation of nerve density and classification into innervation types at the 1 × 1-mm resolution level. Relocation of the classified squares to the original biopsy position enabled transmural quantification and innervation heterogeneity assessment.

RESULTS Coexisting hyperinnervation, hypoinnervation, and denervation were present in all transmural MI-R biopsy sections. The innervation heterogeneity was greatest in the infarct core (median: 0.14; IQR: 0.12-0.15), followed by the border zone (median: 0.05; IQR: 0.04-0.07; $P = 0.02$) and remote zone (median: 0.02; IQR: 0.02-0.03; $P < 0.0001$). Only in the border zone was a positive linear relation between fibrosis and innervation heterogeneity observed ($R = 0.79$; $P < 0.0001$).

CONCLUSIONS This novel method allows quantification of nerve density and heterogeneity in large transmural biopsy sections. In the chronic phase after MI-R, alternating innervation patterns were identified within the same biopsy section. Persistent innervation heterogeneity, in particular in the border zone biopsy sections, may contribute to late arrhythmogenicity. (J Am Coll Cardiol EP 2023;9:1652–1664) © 2023 by the American College of Cardiology Foundation.

From the [a]Department of Cardiology, Willem Einthoven Center for Cardiac Arrhythmia Research and Management, Leiden University Medical Center, Leiden, the Netherlands; [b]Department of Anatomy and Embryology, Leiden University Medical Center, Leiden, the Netherlands; [c]Department of Cell and Chemical Biology, Leiden University Medical Center, Leiden, the Netherlands; and the [d]Department of Cardiology, Willem Einthoven Center for Cardiac Arrhythmia Research and Management, Aarhus University Hospital, Aarhus, Denmark. *Drs Zeppenfeld and Jongbloed contributed equally to this work.

ISSN 2405-500X/$36.00 https://doi.org/10.1016/j.jacep.2023.04.021

The autonomic nervous system plays a crucial role in maintaining intrinsic cardiac functions under physiologic conditions.[1] Acute and chronic changes under pathologic conditions, such as myocardial infarction (MI), may lead to cardiac autonomic dysfunction and have been linked to ventricular arrhythmias and sudden cardiac death.[2-4]

At a histologic level, acute denervation is observed directly after MI, followed by nerve sprouting and hyperinnervation.[4] This is often described as an early phenomenon, but the exact timing and duration remain ambiguous.[5-9] Studies performed at later timepoints (>2 months) are sparse. An increased density of sympathetic nerves in explanted human hearts of transplant recipients, including patients with ischemic heart disease, has been associated with a history of spontaneous ventricular arrhythmias.[10]

In human ischemic heart disease, myocardial nerve fibers seem to regenerate after necrotizing injuries, and some of these scar-associated nerve fibers have structural features visually differing from those in uninjured myocardium.[11] These differences include, among others, a visually greater nerve density in left ventricular scars than in intact myocardium and hypoinnervation or denervation in deeper aspects of the scars. The deeper aspect of the scars is commonly referred to as the infarct core, the area in the vicinity of the scar as the border zone, and areas farther away from the scar as the remote zone. Numerous reports in different animal models have confirmed the occurrence of anomalous innervation patterns after cardiac injury,[6,12-16] mostly in myocardial infarction models with persistent occlusion of a coronary artery. Data from myocardial infarction models with acute reperfusion (MI-R) are scarce,[17,18] which may be relevant because currently most patients in the Western world receive acute reperfusion therapy.[19,20]

Histologic quantification of nerves requires high-resolution images and has proven to be extremely challenging because cardiac nerves are very small and delicate structures. Thus far, most studies mainly focus on quantifying nerve density only in local regions of interest (no transmural evaluation), being presented as the area of nerves divided by the total tissue area.[5,21,22] Comparing the nerve density between diseased and control tissue results in either hyperinnervation or denervation. Only 2 studies have quantified both hyperinnervation and denervation simultaneously.[7,23] Although a solid systematic approach was used in these studies, quantification analyses were primarily based on separate, nontransmural regions of interest to demonstrate hyperinnervation and denervation.

ABBREVIATIONS AND ACRONYMS

MI = myocardial infarction

MI-R = myocardial infarction with reperfusion

In the current study, we aim to contribute to solving these gaps by: 1) developing a novel method to allow the visualization, quantification, and assessment of the heterogeneity of nerve distributions in large transmural biopsy sections; and 2) using this method for the determination of cardiac innervation patterns in a porcine model in the chronic phase of MI-R.

METHODS

ANIMAL MODELS. Approval for the study was obtained from the Danish Animal Experiments Inspectorate (2017-15-0201-01259). All animal procedures complied with local institutional guidelines. In 4 domestic Danish swine (66 ± 2 kg), MI was induced by placing an intravascular balloon after the second diagonal branch of the left anterior descending coronary artery and inflating for 65 minutes, followed by reperfusion.[24] The animals were sacrificed after 3 months. Three fresh abattoir swine hearts were included as controls.

EX VIVO IMAGE INTEGRATION. Sacrifice was performed with potassium chloride during general anesthesia to arrest the heart at the end-diastolic phase to facilitate accurate ex vivo registration with the electroanatomical map. Excised hearts were processed as described previously.[25] Briefly, the chambers were filled with HistOmer (HistOtech) to maintain end-diastolic chamber dimensions and then fixed with 4% formaldehyde.[26] The hearts were subsequently sliced in 5-mm-thick slices (Cater Chef Slicer 300ES-12). Three-dimensional meshes were digitally created from the gross pathologic slices (MASS, research version 2016)[27] (**Figure 1A**). Contours of the endocardium, the aorta, and the 3 ablation lesions were manually traced on the images of the short-axis slices (MASS, research version 2016).[25] The 3-dimensional meshes created from these contours were imported into CARTO 3 version 6.0 (Biosense Webster) and merged with the electroanatomic mapping data using the 3 ablation lesions as landmarks.

The authors attest they are in compliance with human studies committees and animal welfare regulations of the authors' institutions and Food and Drug Administration guidelines, including patient consent where appropriate. For more information, visit the Author Center.

Manuscript received November 28, 2022; revised manuscript received April 5, 2023, accepted April 21, 2023.

FIGURE 1 Workflow Overview

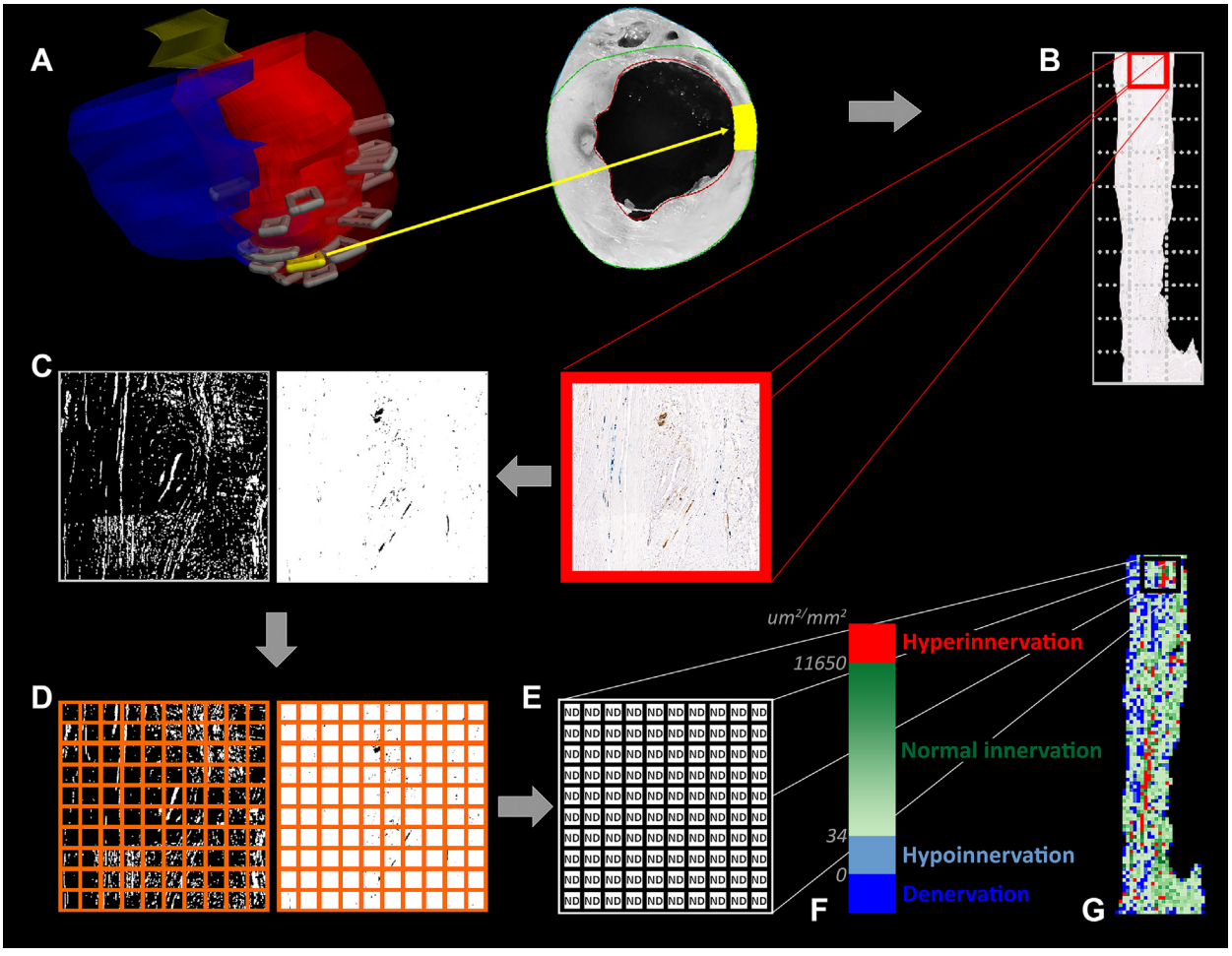

(A) The 3-dimensional location of the biopsies. **(B)** Immunohistochemically stained sections exported in a 1 × 1-mm grid. **(C)** Thresholded nerve and myocardial tissue masks with quality check and removal of endocardium, epicardium, and artifacts. **(D)** Division into 0.1 × 0.1-mm squares. **(E)** Calculation of the nerve densities in each square. **(F)** Classification into the innervation type. **(G)** Relocation into the original position within the biopsy section.

The registration matrix, mapping point coordinates, and voltages were exported from CARTO 3. Using inverse registration, all points were superimposed on the pathology slices and projected onto the closest contour (MATLAB, release 2015b, MathWorks Inc). Points that had to be translocated ≥10 mm from the CARTO map to be projected onto a gross pathology contour were excluded. Transmural biopsy sections with a height of 10 mm were taken throughout the left ventricle, corresponding with previously obtained biopsy sections for histologic analysis of fibrosis patterns based on electroanatomic voltage-mapping sites[24] (Supplemental Methods, Supplemental Figure 1). Biopsy sections from the control swine were taken at similar locations as those from the experimental swine.

(IMMUNO)HISTOCHEMISTRY. Biopsy sections were embedded in paraffin and sectioned at a thickness of 7 μm. Sections were stained with picrosirius red with Weigert's hematoxylin counterstaining to visualize collagen and viable myocardium. Autonomic nerves were visualized using anti-beta-III tubulin 3-3′-diaminobenzidine tetrahydrochloride staining (Sigma Aldrich). To conceal the intrinsically brown iron deposits in macrophages, known to be present after MI with reperfusion,[28] Prussian blue staining was performed on the sections after anti-beta-III tubulin

FIGURE 2 Calculation of the Innervation Heterogeneity

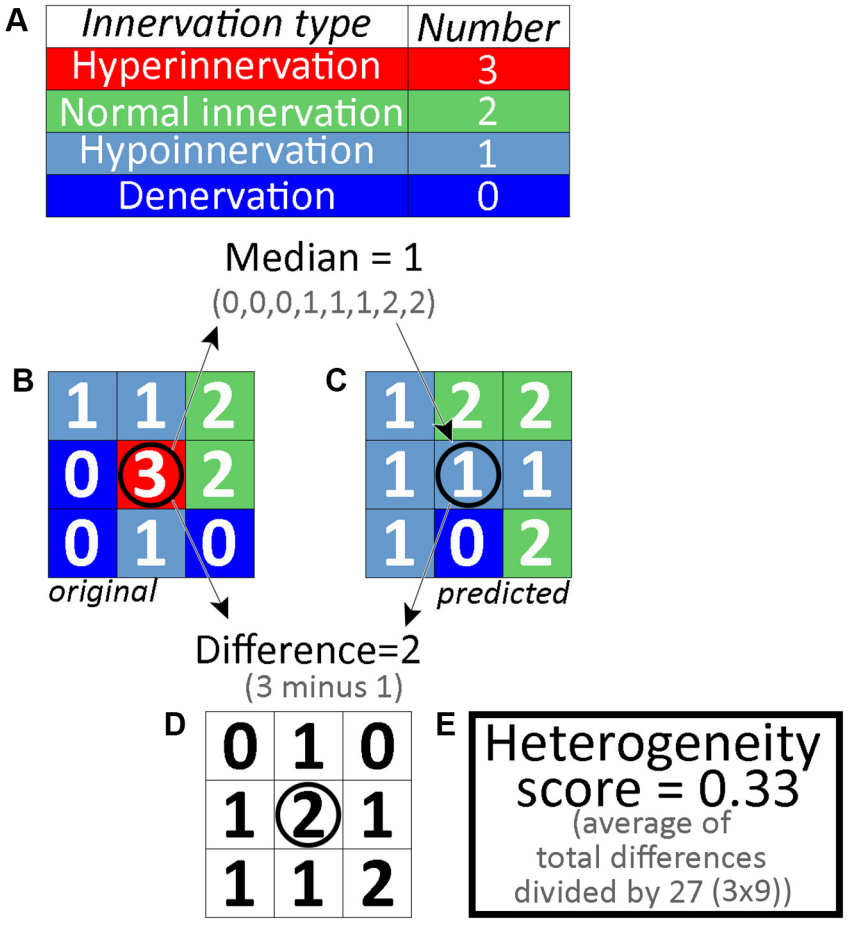

(A) Assigned number per innervation type. **(B)** Extraction of the numbers from all neighboring squares (original input). **(C)** Calculated predicted value (median of the neighboring squares). **(D)** Calculated difference between the original and predicted values. **(E)** Calculation of the heterogeneity score: the grid sum divided by the maximal grid score (**squares** multiplied by maximum difference: $9 \times 3 = 27$).

staining of the myocardium (Supplemental Figure 2).[29] Detailed descriptions are provided in the Supplemental Methods.

DIGITAL MICROSCOPY. Sections were digitally scanned at 40× magnification (Panoramic 250 Flash III, 3DHistech Ltd) and stored as MRXS files.

QUANTITATIVE ANALYSES. Export. Using a custom MATLAB script, the MRXS files could be imported, and each scanned biopsy section was graphically divided into a 1×1-mm grid. Each 1×1-mm tile could subsequently be exported to a TIFF file to maintain the image resolution (Figure 1B).

Fibrosis and viable myocardium. The proportion of fibrosis and the amount of viable myocardium was calculated in each transmural biopsy section as previously described.[27] Fibrosis cutoffs were used to classify the biopsy sections into MI core (>59.8% fibrosis), border zone (14.3%-59.8% fibrosis) or remote zone (<14.3% fibrosis).[24]

Nerve density visualization and quantification. With a custom ImageJ macro (National Institutes of Health), the tiles were automatically color deconvoluted, and nerve masks were automatically created using these color deconvoluted tiles (threshold: 0-155) after the subtraction of iron (threshold: 0-160). The threshold was determined manually on the background staining of the original tiles for each biopsy section to automatically create myocardial tissue masks (Figure 1C). Next, each original tile with corresponding nerve and myocardial tissue masks was opened for a quality check and removal of artifacts and epicardium in a

TABLE 1 Histologic Characteristics Categorized by Biopsy Groups

	Core (n = 9)	Border Zone (n = 30)	Remote (n = 44)	*P* Value
Wall thickness, mm	2.2 ± 0.4	6.3 ± 2.6	9.2 ± 2.4	<0.0001
Fibrosis, %	73.0 (70.3-74.7)	33.6 (22.3-42.6)	8.5 (7.2-9.7)	<0.0001
Viable myocardium, mm^2	5.4 (3.6-6.7)	39.8 (22.8-56.1)	76.4 (62.0-93.4)	<0.0001

Values are mean ± SD or median (IQR).

semiautomatic fashion. The endocardium and epicardium were removed because they were not consistently preserved in all biopsy sections. Examples of an ideal and average section are provided in the supplemental materials (Supplemental Figure 3). Because myocardial tissue masks were based on background staining, they were filtered to ensure an equal distribution throughout the biopsy section. Further division into 0.1 × 0.1-mm squares was achieved using a custom Python script (Python Software Foundation), and nerve density per square ($\mu m^2/mm^2$) was calculated and classified into innervation types according to cutoffs derived from the control swine (5th and 95th percentiles: <34 $\mu m^2/mm^2$ and >11,650 $\mu m^2/mm^2$, respectively; n = 38 biopsy sections) (**Figures 1D to 1F**). Finally, squares were located back to their original position within the biopsy section, allowing visualization of the different innervation types within 1 biopsy section (**Figure 1G**). The percentage of different innervation types within each biopsy section was then calculated by dividing the area of each innervation type by the total biopsy section area. The accuracies of the nerve density and tile size to discriminate differences in the original stained biopsy section were visually validated (Supplemental Figure 4).

Nerve density heterogeneity. To calculate the nerve density heterogeneity within each biopsy section, the 0.1 × 0.1-mm squares received a value according to the innervation type: 0 for denervation, 1 for hypoinnervation, 2 for normal innervation, and 3 for hyperinnervation (**Figure 2A**). The method to determine the heterogeneity score was inspired by the median filter technique, which is widely used in digital image processing.[30] In short, for each individual square, the values of the neighboring squares were taken, and the median of these values represented the predicted value (**Figures 2B and 2C**). Subsequently, the difference between the predicted value and original value of each square was scored (**Figure 2D**). The heterogeneity score was determined by averaging all scores and dividing by the maximal possible score (total number of squares multiplied by 3) (**Figure 2E**). The heterogeneity score ranges from 0 (homogeneous) to 1 (maximally heterogeneous). Wider radiuses can be applied to assess the heterogeneity based on a broader environment within the biopsy section (Supplemental Figure 5).

STATISTICAL ANALYSIS. Continuous variables are reported as mean ± SD for normal distributed data or median (IQR) for data with nonnormal distribution. Categorical data are presented as number (percentage). Data were analyzed by means of Spearman correlation, 1-way analysis of variance test (normal distribution), or Kruskal-Wallis test (nonnormal distribution) for multigroup comparison followed by Dunn's post hoc test for pairwise comparison when appropriate. Statistical analyses were performed with GraphPad Prism version 6.07 (GraphPad Inc) or RStudio version 1.4.1717 (RStudio). A value of $P < 0.05$ was considered statistically significant.

RESULTS

VISUALIZATION AND ANALYSIS OF INNERVATION WITHIN INDIVIDUAL BIOPSY SECTIONS. A total of 83 transmural MI-R biopsy sections were taken, with a median of 21[19-23] biopsy sections per heart. Of these, 9 were classified as core infarct, 30 as infarct border zone, and 44 as remote myocardium according to the percentage of fibrosis. Classification according to the electroanatomic voltage map showed similar results (Supplemental Figure 6). **Table 1** provides the descriptive statistics per group.

After quantification, different innervation types could be visualized within each transmural biopsy section (**Figure 3**).

QUANTIFICATION OF INNERVATION TYPES. Several coexisting innervation patterns were observed in the infarct core and border zone (**Figure 4A**). Hyperinnervation was observed mainly in the border zone (median: 5.3%; IQR: 3.7%-9.4%) and, remarkably, also in the core infarct (median: 5.3%; IQR: 3.7%-9.4%; P = >0.99), while it was low in remote myocardium (median: 2.6%; IQR: 1.7%-4.3%; $P = 0.002$ and $P = 0.038$, respectively) (**Figure 4B**). Normal innervation was mostly observed in remote myocardium (median: 94.9%; IQR: 93.8%-96.0%), was decreased in the border zone (median: 87.9%; IQR: 85.1%-92.4%; $P < 0.001$), and was lowest in the core infarct (median: 72.8%; IQR: 66.3%-75.8%; $P < 0.001$) (**Figure 4C**). The percentages of hypoinnervation and denervation per biopsy section were highest in the infarct core (hypoinnervation: median: 3.8%; IQR: 2.9%-5.0%; denervation: median: 16.7%;

FIGURE 3 Visualization of Innervation Within an Individual Biopsy Section

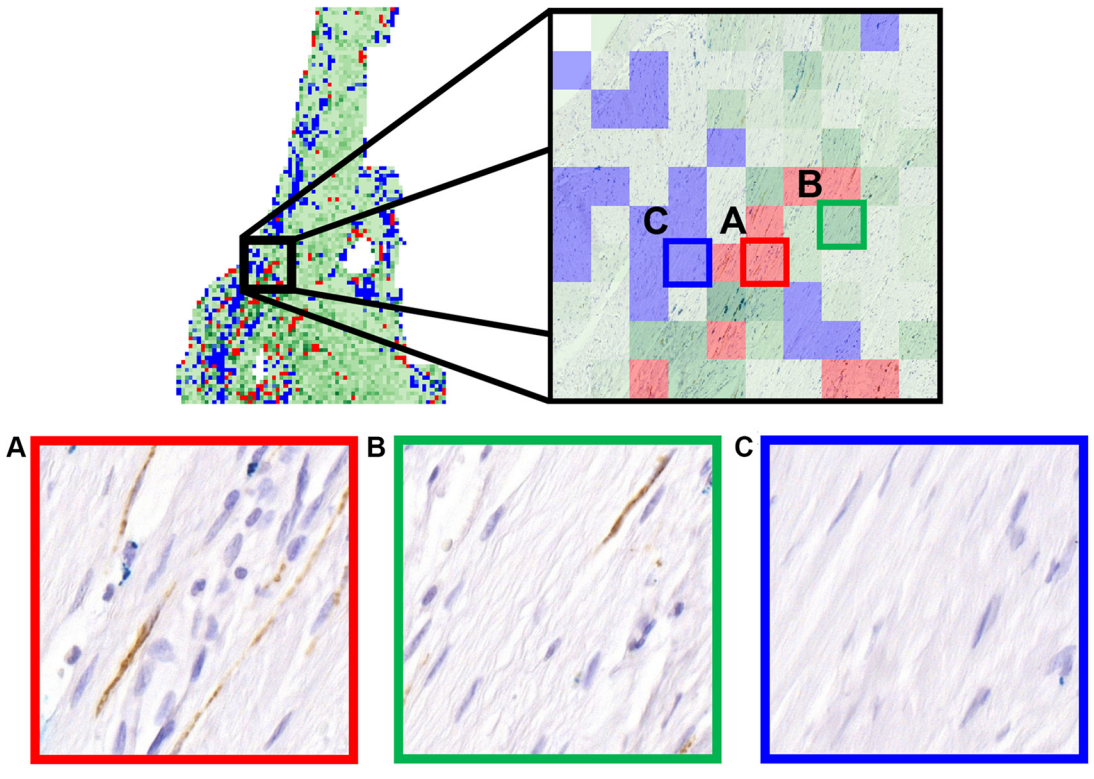

Different innervation types visualized within 1 transmural biopsy section: **(A)** hyperinnervation, **(B)** normal innervation, and **(C)** denervation.

IQR: 13.5%-23.5%), lower in the border zone (hypoinnervation: median: 1.2%; IQR: 0.8%-1.7%; $P = 0.015$; denervation: median: 2.6%; IQR: 1.6%-6.5%; $P = 0.008$), and lowest in the remote myocardium (hypoinnervation: median: 0.6%; IQR: 0.3%-1.3%; $P < 0.001$; denervation: median: 1.2%; IQR: 0.7%-1.8%; $P < 0.001$) (Figures 4D and 4E). In the examples presented in Figure 5, denervation and hypoinnervation could be observed in the subendocardial region, coinciding with compact fibrotic scar, whereas hyperinnervation was observed in the adjacent midmyocardial and subepicardial regions in the core and border zone biopsy sections. The hyperinnervated autonomic nerves were mainly of sympathetic origin (Supplemental Figure 7).

HETEROGENEOUS INNERVATION AS RELATED TO FIBROSIS AND VIABLE MYOCARDIUM. Three months after MI-R, innervation was most heterogeneous in the core biopsy sections (median: 0.14; IQR: 0.12-0.15), less heterogeneous in the border zone (median: 0.05; IQR: 0.04-0.07; $P = 0.02$), and most homogeneous in the remote myocardium (median: 0.02; IQR: 0.02-0.03; $P < 0.0001$) (Figure 6A). The amount of viable myocardium was severely reduced in the core (median: 5.4 mm^2; IQR: 3.6-6.7 mm^2), was higher in the border zone (median: 39.8 mm^2; IQR: 22.8-56.1 mm^2; $P = 0.02$), and was highest in the remote zone (median: 76.4 mm^2; IQR: 62.0-93.4 mm^2; $P < 0.0001$) (Figure 6B). Next, the relationship between fibrosis and innervation heterogeneity was examined. Only in border zone biopsy sections did the heterogeneity show a linear increase with the percentage of fibrosis ($R = 0.79$; $P < 0.0001$) (Figure 6C). The linear relationship between fibrosis and heterogeneity was absent in remote myocardium ($R = 0.23$; $P = 0.14$) and core infarct biopsy sections ($R = 0.38$; $P = 0.31$). Similar results were acquired when using a larger radius for the determination of innervation heterogeneity (Supplemental Figure 8).

DISCUSSION

In recent years, there is an increasing interest in the role of disturbed autonomic cardiac innervation patterns in arrhythmogenesis after cardiac injury, such as

FIGURE 4 **Innervation Changes of the Core, Border Zone, and Remote Zone After Myocardial Infarction With Reperfusion**

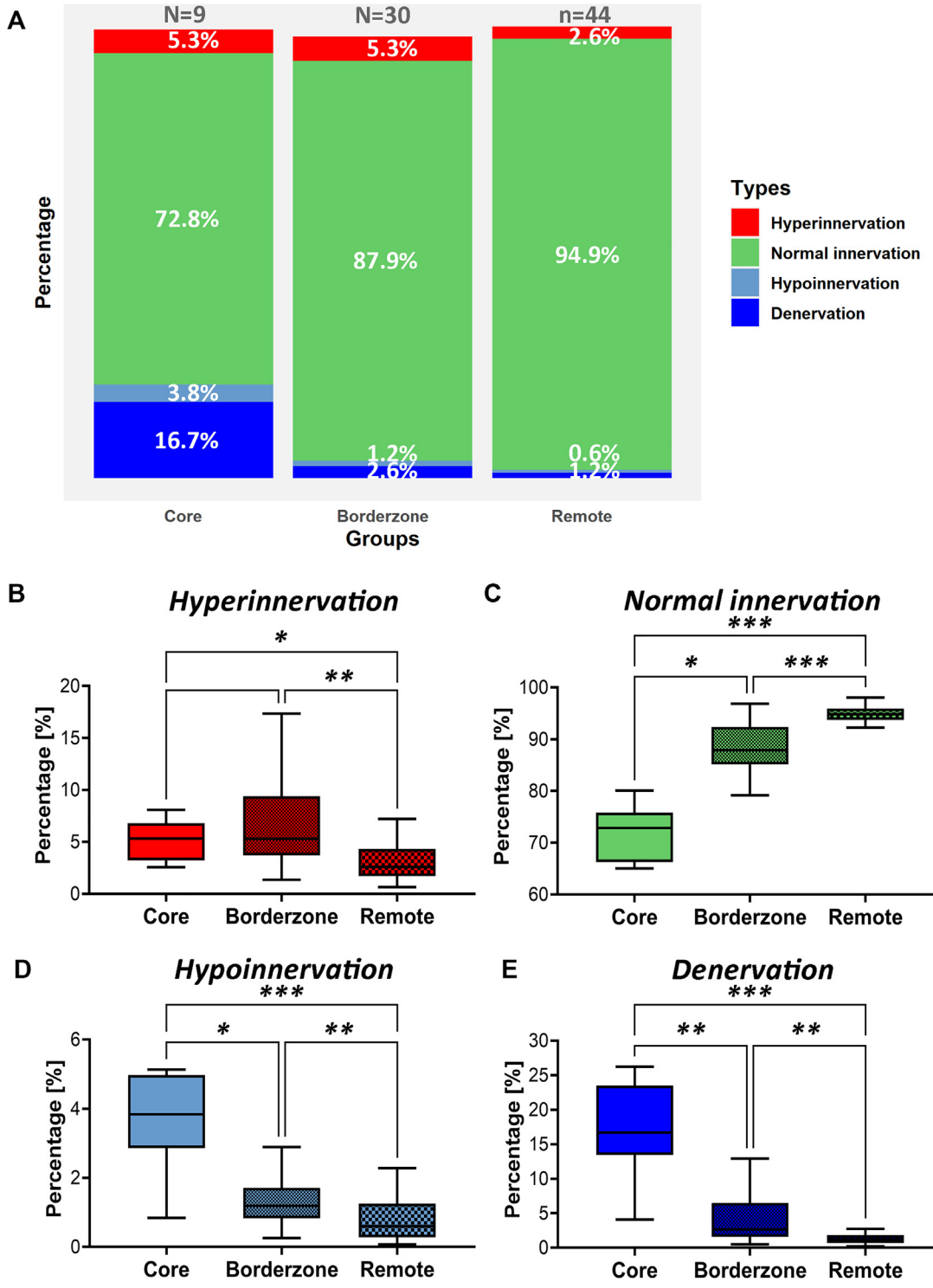

(A) Median percentages of innervation types categorized by group. **(B)** Hyperinnervation is significantly increased in the core and border zone, whereas it is lower in the remote zone. **(C)** Normal innervation is highest in the remote biopsy sections, significantly decreased in the border zone, and lowest in the infarction core. **(D)** Hypoinnervation is significantly increased in the border zone and core compared to remote biopsy sections. **(E)** The percentage of denervation is highest in the infarction core, lower in the border zone, and lowest in the remote biopsy sections. *$P < 0.05$, **$P < 0.01$, ***$P < 0.0001$.

FIGURE 5 Representative Examples of Analyzed Biopsy Sections

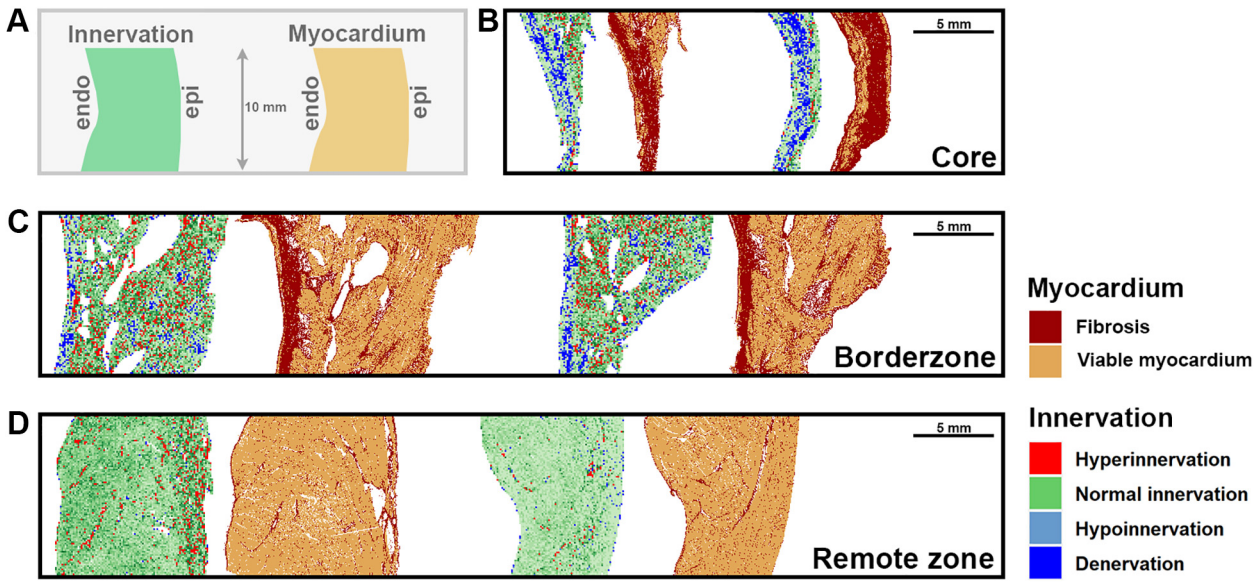

(A) Legend. **(B)** Core biopsy examples. **(C)** Border zone biopsy examples. **(D)** Remote zone biopsy examples. endo: endocardium; epi: epicardium.

MI. In this study, we use a novel workflow to provide histologic evaluation and quantification of nerve density and heterogeneity across large transmural biopsy sections in an MI-R model (**Central Illustration**). This workflow leverages the advantages of existing freely available software. To the best of our knowledge, such an analysis has never been performed to date. The key results of the study are as follows:

- Visualization and quantification of different innervation types within large transmural biopsy sections could be achieved.
- In a chronic porcine MI-R model, denervation, hypoinnervation, and hyperinnervation coexisted in transmural core and border zone biopsy sections.
- The heterogeneity in innervation showed a linear increase with the amount of fibrosis in the infarct border zone.

SPATIAL DISTRIBUTION OF INNERVATION WITHIN LARGE TRANSMURAL BIOPSY SECTIONS AND ITS RELATION WITH FIBROSIS. Early reperfusion is currently the standard treatment of myocardial infarction and results in smaller and inhomogeneous fibrotic scars in the subendocardium extending toward the midmyocardium.[31,32] Denervation in the core and nerve sprouting in the border zone have often separately been mentioned but not quantified.[1,11,33,34] To date, most data in animal studies are derived from MI rodent models without reperfusion. In the current study, the different innervation types were assessed throughout the entire transmural biopsy in a porcine MI-R model from infarct core, border zone, and remote zone. Because healthy large animals and humans have predominantly vagal tone, whereas small rodents have predominantly sympathetic tone,[35] this large animal model may be more representative of human autonomic innervation than prior rodent models. This method can potentially be applied to human biopsy sections (Supplemental Figure 9).

CHANGES OF INNERVATION PATTERNS IN CHRONIC MI-R. Our finding of hyperinnervation in the border zone is in agreement with several other studies in different animal models.[5,8,36-38] In contrast, our findings are based on the quantification of hyperinnervation in the entire transmural biopsy section rather than showing an increased nerve density in a region of interest. Surprisingly, in the current study, hyperinnervation was also present in the infarct core. This finding may partly be attributed to our definition of the core infarct and border zone. The transmural biopsy sections in the present study were classified according to cutoffs in the percentage of fibrosis and, in addition, according to electroanatomic voltage mapping, which showed similar results (as presented in the supplemental materials). As a consequence,

FIGURE 6 Differences in Innervation Heterogeneity and Viable Myocardium Within the Infarction Core, Border Zone, and Remote Zone

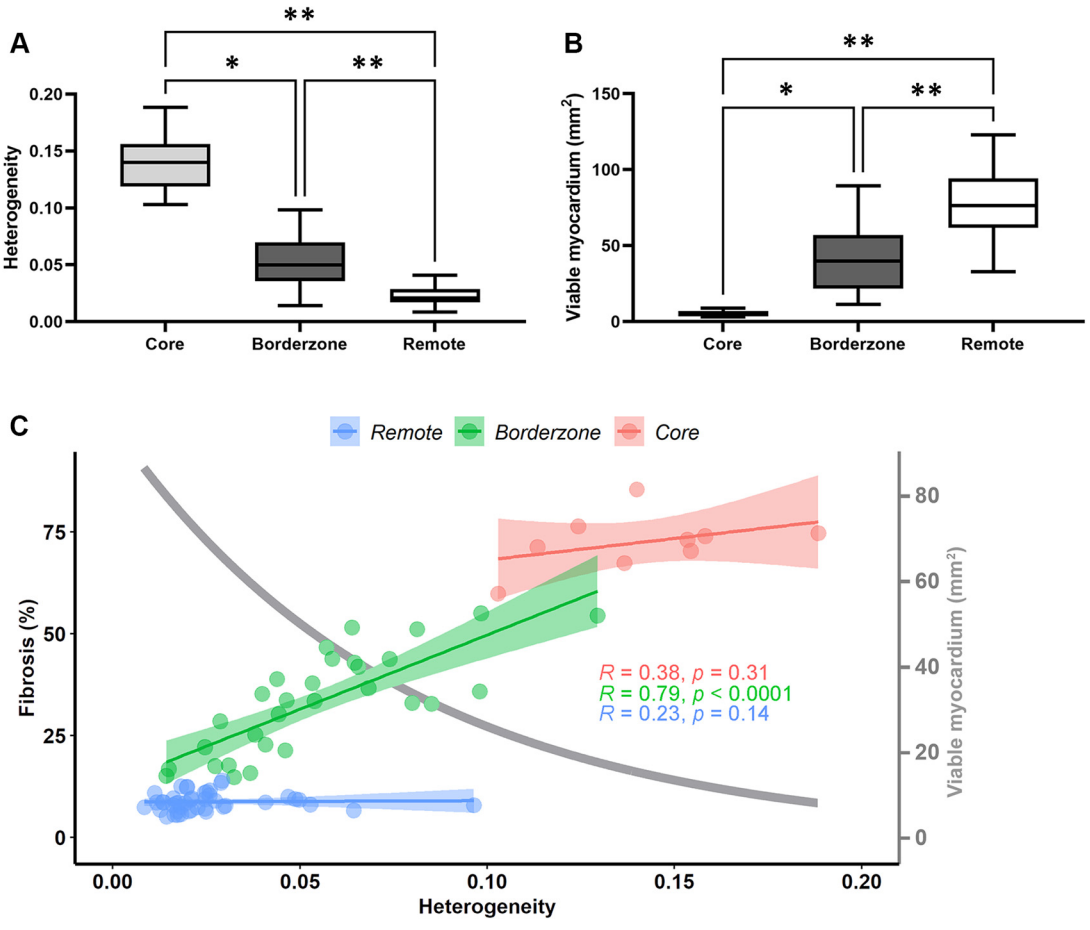

(A) Innervation heterogeneity is highest in the core, lower in the border zone, and lowest in the remote zone. **(B)** The amount of viable myocardium is highest in the remote zone, partially preserved in the border zone, and severely reduced in the core. **(C)** A significant increase in innervation heterogeneity is observed with increasing fibrosis in the border zone biopsy sections. No significant association between innervation heterogeneity and fibrosis is found in the remote and core biopsy sections. The gray line illustrates the viable myocardium in relation to the heterogeneity. *$P < 0.05$, **$P < 0.0001$.

transmural biopsy sections could include areas with dense fibrosis but also areas with diffuse fibrosis or viable myocardium. Because previous studies relied on the histologic quantification of the nerve density within regions of interest, it is imaginable that a region is classified as border zone when being directly localized next to an area of dense fibrosis. Besides sympathetic hyperinnervation, other changes in innervation may occur after MI. Denervation and hypoinnervation were moderately increased in the border zone but markedly present in the infarction core in our MI-R model, supporting the findings of preceding studies and validating the novel quantitative method presented in the current study.[7,11,34,37]

SUBSTRATE HETEROGENEITY. Ventricular arrhythmias after MI are often caused by re-entry mechanisms. Heterogenous and slow conduction in the border zone with activation proceeding along pathways lengthened by branching and merging bundles of viable myocardium separated by collagenous septa is one crucial requirement for re-entry to occur.[39] In addition, large transitions in border zone thickness can form regions of functional conduction block, further contributing to the ventricular tachycardia substrate.[40] Components in this concept are myocardium and scar fibroblasts, whereas the potential role of nerve sprouting after MI(-R) currently is not considered critical. Interestingly, the

CENTRAL ILLUSTRATION **Overview of the Study**

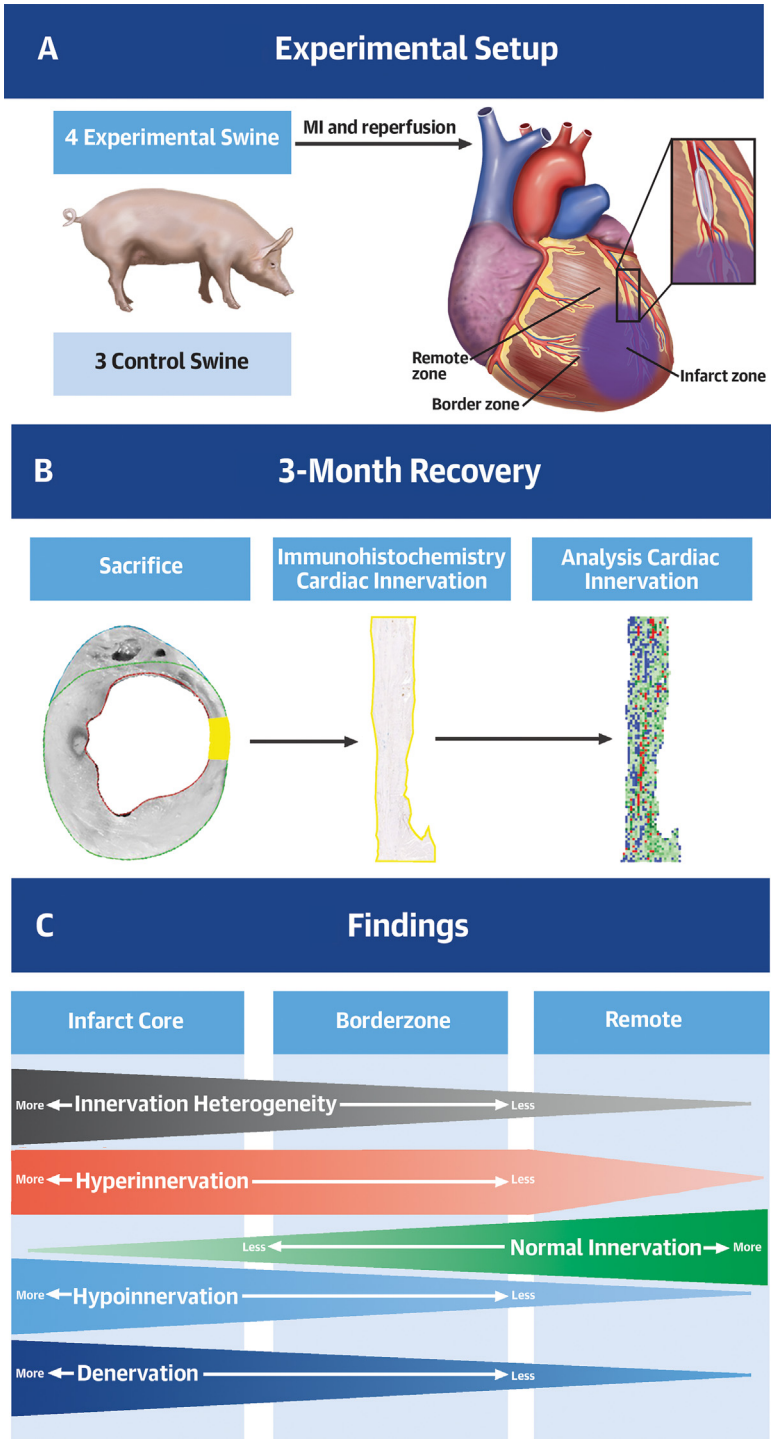

Chen H.S, et al. J Am Coll Cardiol EP. 2023;9(8):1652-1664.

(A) Induction of myocardial infarction by intravascular balloon inflation in the left anterior descending coronary artery followed by reperfusion. **(B)** Extraction of the hearts, immunohistochemical staining, and analysis of cardiac innervation. **(C)** Differences in innervation heterogeneity and innervation types in the infarct core, border zone, and remote biopsy sections.

heterogeneity of repolarization can be aggravated by sympathetic stimulation.[41] Upon sympathetic stimulation, in patients without cardiomyopathy, all regions of the heart significantly and uniformly exhibit shortening of the activation recovery interval, a reliable surrogate for the action potential duration. In contrast, a significant variation in response to sympathetic stimulation has been observed in the hearts of patients with ischemic cardiomyopathy, even within the same regions of the border zone.[41] Similarly, in a porcine model of anteroapical MI-R, sympathetic stimulation induced heterogeneous changes on activation and even paradoxically prolonged activation propagation at some border zone sites.[42]

The finding in the present study of a positive association between innervation heterogeneity and fibrosis—while, naturally, a reversed relation was observed with the amount of viable myocardium—may in part account for the dynamic nature of the responses to sympathetic stimulation in the border zone and the predisposition to ventricular arrhythmias after MI-R.

SYMPATHETIC HYPERINNERVATION. The majority of the nerve fibers involved in regional left ventricular hyperinnervation after MI are sympathetic nerves (Supplemental Figure 5).[10] Parasympathetic nerve fibers innervate the left ventricle as well, but to a much lesser extent.[43,44] The role and potential alterations of parasympathetic nerves after MI are poorly studied and remain controversial. A greater quantity of parasympathetic nerve fibers has been reported to be increased in the border zone and infarct zone than in the remote zone,[45] whereas others have documented no parasympathetic hyperinnervation.[5] Adding to this complexity, evidence suggests that MI can cause cholinergic transdifferentiation of sympathetic nerves.[46]

Therefore, the contribution of sympathetic innervation in arrhythmogenicity after MI seems to be undeniable, but the role of parasympathetic cardiac innervation and the interplay between both systems remains largely unclear and warrants further investigation.

STUDY LIMITATIONS. Fiber orientation may influence nerve density—eg, a longitudinal orientation leads to a higher nerve density than a cross-sectional orientation, which is difficult to solve because the structure of the myocardium (with its innervation) is normally oriented in multiple directions.[47] However, by taking the entire transmural biopsy section into account and not a localized area of the myocardial wall, the presented method eliminates a substantial influence of fiber orientation on the results. Additionally, prior research on noninfarcted swine hearts found no discernible variations between the subepicardium, midmyocardium, and subendocardium layers.[48]

Classification of the nerve density into the different innervation types was based on cutoff values identified in control swine. These values may show interspecies differences and therefore need to be validated in other species.

The study focused on a postinfarct model using distal left anterior descending coronary artery occlusion followed by reperfusion. Because nerve density shows regional differences in the heart, the results may differ in other MI locations than anterior wall infarctions.

CONCLUSIONS

Here, we present a novel workflow for the visualization and quantification of nerve density and heterogeneity of large transmural biopsy sections in the chronic phase after MI-R. This workflow, which is based on existing freely available software packages and platforms, has the potential to be broadly applied to any research involving high-resolution imaging of nerves in large tissues. It enables the histologic study of the location of denervation and hyperinnervation after MI-R and may also be applied to human biopsy sections. In our chronic porcine MI-R model, coexisting areas of different innervation patterns were identified within individual biopsy sections. Combined with persisting viable myocardium in the border zone, this may form a potentially heterogeneous substrate for arrhythmias.

ACKNOWLEDGMENT The authors gratefully acknowledge Prof Dr V.T.H.B.M. Smit for identifying iron deposits in macrophages in our biopsy sections.

FUNDING SUPPORT AND AUTHOR DISCLOSURES

Dr Jongbloed is supported by a personal research grant from NWO ZonMw (project no. 91719346), by a grant of the Dutch Bontius Stichting, and by a grant from the Rembrandt Foundation. Marco DeRuiter is funded by the Dutch Heart Foundation and by a grant of the Dutch Bontius Stichting. All other authors have reported that they have no relationships relevant to the contents of this paper to disclose.

ADDRESS FOR CORRESPONDENCE: Dr Monique R.M. Jongbloed, Center for Congenital Heart Disease Amsterdam-Leiden (CAHAL), Department of Cardiology and Anatomy and Embryology, Leiden University Medical Center, Postal zone: S-1-P, PO Box 9600, 2300 RC Leiden, the Netherlands. E-mail: m.r.m.jongbloed@lumc.nl.

PERSPECTIVES

COMPETENCY IN MEDICAL KNOWLEDGE: Cardiac innervation is important in arrhythmogenicity but difficult to analyze because of the small size of cardiac nerves. For the first time, to our knowledge, a workflow to histologically analyze cardiac innervation in large transmural biopsy sections is described in this article.

TRANSLATIONAL OUTLOOK: Combining transmural histologic cardiac innervation data with electrophysiologic parameters such as conduction velocity and regional action potential duration in future studies may provide new insights in pathologic cardiac innervation in relation to the substrate for ventricular arrhythmias. Future studies evaluating the potential consequences for autonomic neuromodulation will aid in the development of novel arrhythmia treatments for chronic myocardial infarction.

REFERENCES

1. Goldberger JJ, Arora R, Buckley U, Shivkumar K. Autonomic nervous system dysfunction: *JACC* focus seminar. *J Am Coll Cardiol*. 2019;73:1189–1206.

2. Fukuda K, Kanazawa H, Aizawa Y, Ardell JL, Shivkumar K. Cardiac innervation and sudden cardiac death. *Circ Res*. 2015;116:2005–2019.

3. Boogers MJ, Borleffs CJ, Henneman MM, et al. Cardiac sympathetic denervation assessed with 123-iodine metaiodobenzylguanidine imaging predicts ventricular arrhythmias in implantable cardioverter-defibrillator patients. *J Am Coll Cardiol*. 2010;55:2769–2777.

4. Vaseghi M, Shivkumar K. The role of the autonomic nervous system in sudden cardiac death. *Prog Cardiovasc Dis*. 2008;50:404–419.

5. Oh YS, Jong AY, Kim DT, et al. Spatial distribution of nerve sprouting after myocardial infarction in mice. *Heart Rhythm*. 2006;3:728–736.

6. Drobysheva A, Ahmad M, White R, Wang HW, Leenen FH. Cardiac sympathetic innervation and PGP9.5 expression by cardiomyocytes after myocardial infarction: effects of central MR blockade. *Am J Physiol Heart Circ Physiol*. 2013;305:H1817–H1829.

7. Lorentz CU, Parrish DC, Alston EN, et al. Sympathetic denervation of peri-infarct myocardium requires the p75 neurotrophin receptor. *Exp Neurol*. 2013;249:111–119.

8. Zhou S, Chen LS, Miyauchi Y, et al. Mechanisms of cardiac nerve sprouting after myocardial infarction in dogs. *Circ Res*. 2004;95:76–83.

9. Zhao S, Dai Y, Ning X, et al. Vagus nerve stimulation in early stage of acute myocardial infarction prevent ventricular arrhythmias and cardiac remodeling. *Front Cardiovasc Med*. 2021;8:648910.

10. Cao JM, Fishbein MC, Han JB, et al. Relationship between regional cardiac hyperinnervation and ventricular arrhythmia. *Circulation*. 2000;101:1960–1969.

11. Vracko R, Thorning D, Frederickson RG. Nerve fibers in human myocardial scars. *Hum Pathol*. 1991;22:138–146.

12. Gu Y, Wang X, Wu G, et al. Artemisinin suppresses sympathetic hyperinnervation following myocardial infarction via anti-inflammatory effects. *J Mol Histol*. 2012;43:737–743.

13. Hu H, Xuan Y, Xue M, et al. Semaphorin 3A attenuates cardiac autonomic disorders and reduces inducible ventricular arrhythmias in rats with experimental myocardial infarction. *BMC Cardiovasc Disord*. 2016;16:16.

14. Amino M, Yoshioka K, Tanaka S, et al. Normal (123) I-MIBG uptake areas may be associated with hyperinnervation and arrhythmia risk in phenol model rabbit hearts. *Pacing Clin Electrophysiol*. 2017;40:1103–1112.

15. Chen T, Cai MX, Li YY, et al. Aerobic exercise inhibits sympathetic nerve sprouting and restores beta-adrenergic receptor balance in rats with myocardial infarction. *PLoS One*. 2014;9:e97810.

16. Wernli G, Hasan W, Bhattacherjee A, van Rooijen N, Smith PG. Macrophage depletion suppresses sympathetic hyperinnervation following myocardial infarction. Basic Res. *Cardiol*. 2009;104:681–693.

17. Gardner RT, Habecker BA. Infarct-derived chondroitin sulfate proteoglycans prevent sympathetic reinnervation after cardiac ischemia-reperfusion injury. *J Neurosci*. 2013;33:7175–7183.

18. Pellegrino MJ, Habecker BA. STAT3 integrates cytokine and neurotrophin signals to promote sympathetic axon regeneration. *Mol Cell Neurosci*. 2013;56:272–282.

19. Ibanez B, James S, Agewall S, et al. 2017 ESC Guidelines for the management of acute myocardial infarction in patients presenting with ST-segment elevation: the Task Force for the Management of Acute Myocardial Infarction in Patients Presenting With ST-Segment Elevation of the European Society of Cardiology (ESC). *Eur Heart J*. 2018;39:119–177.

20. Levine GN, Bates ER, Blankenship JC, et al. 2015 ACC/AHA/SCAI focused update on primary percutaneous coronary intervention for patients with ST-elevation myocardial infarction: an update of the 2011 ACCF/AHA/SCAI Guideline for Percutaneous Coronary Intervention and the 2013 ACCF/AHA Guideline for the Management of ST-Elevation Myocardial Infarction. *J Am Coll Cardiol*. 2016;67:1235–1250.

21. Liu Q, Chen D, Wang Y, Zhao X, Zheng Y. Cardiac autonomic nerve distribution and arrhythmia. *Neural Regen Res*. 2012;7:2834–2841.

22. Wang Y, Shao C, Qi L, et al. EphrinB2-RhoA upregulation attenuates sympathetic hyperinnervation and decreases the incidence of ventricular arrhythmia after myocardial infarction. *J Cardiol*. 2022;79:423–431.

23. Yokoyama T, Lee JK, Miwa K, et al. Quantification of sympathetic hyperinnervation and denervation after myocardial infarction by three-dimensional assessment of the cardiac sympathetic network in cleared transparent murine hearts. *PLoS One*. 2017;12:e0182072.

24. Glashan CA, Tofig BJ, Tao Q, et al. Multisize electrodes for substrate identification in ischemic cardiomyopathy: validation by integration of whole heart histology. *J Am Coll Cardiol EP*. 2019;5:1130–1140.

25. Glashan CA, Tofig BJ, Tao Q, et al. Whole heart histology: a method for the direct integration of histology with electrophysiological and imaging data. *J Am Coll Cardiol EP*. 2020;6:461–462.

26. Bjarkam CR, Pedersen M, Sorensen JC. New strategies for embedding, orientation and sectioning of small brain specimens enable direct correlation to MR-images, brain atlases, or use of

unbiased stereology. *J Neurosci Methods*. 2001;108:153–159.

27. Glashan CA, Androulakis AFA, Tao Q, et al. Whole human heart histology to validate electroanatomical voltage mapping in patients with non-ischaemic cardiomyopathy and ventricular tachycardia. *Eur Heart J*. 2018;39:2867–2875.

28. Kali A, Kumar A, Cokic I, et al. Chronic manifestation of postreperfusion intramyocardial hemorrhage as regional iron deposition a cardiovascular magnetic resonance study with ex vivo validation. *Circ Cardiovasc Imaging*. 2013;6:218–228.

29. Bancroft JD, Stevens A. *Theory and Practice of Histological Techniques*. 2nd ed. Churchill Livingstone; 1982.

30. Huang TS, Yang GJ, Tang GY. Fast 2-dimensional median filtering algorithm. *IEEE Trans Acoust Speech Signal Process*. 1979;27:13–18.

31. Wijnmaalen AP, Schalij MJ, von der Thusen JH, Klautz RJ, Zeppenfeld K. Early reperfusion during acute myocardial infarction affects ventricular tachycardia characteristics and the chronic electroanatomic and histological substrate. *Circulation*. 2010;121:1887–1895.

32. Miyazaki S, Fujiwara H, Onodera T, et al. Quantitative analysis of contraction band and coagulation necrosis after ischemia and reperfusion in the porcine heart. *Circulation*. 1987;75:1074–1082.

33. Chen LS, Zhou S, Fishbein MC, Chen PS. New perspectives on the role of autonomic nervous system in the genesis of arrhythmias. *J Cardiovasc Electrophysiol*. 2007;18:123–127.

34. Barber MJ, Mueller TM, Henry DP, Felten SY, Zipes DP. Transmural myocardial infarction in the dog produces sympathectomy in noninfarcted myocardium. *Circulation*. 1983;67:787–796.

35. Janssen BJ, Smits JF. Autonomic control of blood pressure in mice: basic physiology and effects of genetic modification. *Am J Physiol Regul Integr Comp Physiol*. 2002;282:R1545–R1564.

36. Hasan W, Jama A, Donohue T, et al. Sympathetic hyperinnervation and inflammatory cell NGF synthesis following myocardial infarction in rats. *Brain Res*. 2006;1124:142–154.

37. Li W, Knowlton D, Van Winkle DM, Habecker BA. Infarction alters both the distribution and noradrenergic properties of cardiac sympathetic neurons. *Am J Physiol Heart Circ Physiol*. 2004;286:H2229–H2236.

38. Ajijola OA, Yagishita D, Patel KJ, et al. Focal myocardial infarction induces global remodeling of cardiac sympathetic innervation: neural remodeling in a spatial context. *Am J Physiol Heart Circ Physiol*. 2013;305:H1031–H1040.

39. de Bakker JM, van Capelle FJ, Janse MJ, et al. Slow conduction in the infarcted human heart. 'Zigzag' course of activation. *Circulation*. 1993;88:915–926.

40. Stevenson WG, Friedman PL, Sager PT, et al. Exploring postinfarction reentrant ventricular tachycardia with entrainment mapping. *J Am Coll Cardiol*. 1997;29:1180–1189.

41. Vaseghi M, Lux RL, Mahajan A, Shivkumar K. Sympathetic stimulation increases dispersion of repolarization in humans with myocardial infarction. *Am J Physiol Heart Circ Physiol*. 2012;302:H1838–H1846.

42. Ajijola OA, Lux RL, Khahera A, et al. Sympathetic modulation of electrical activation in normal and infarcted myocardium: implications for arrhythmogenesis. *Am J Physiol Heart Circ Physiol*. 2017;312:H608–H621.

43. Kawano H, Okada R, Yano K. Histological study on the distribution of autonomic nerves in the human heart. *Heart Vessels*. 2003;18:32–39.

44. Pauziene N, Rysevaite-Kyguoliene K, Alaburda P, et al. Neuroanatomy of the pig cardiac ventricles. A stereomicroscopic, confocal and electron microscope study. *Anat Rec (Hoboken)*. 2017;300:1756–1780.

45. Liao SY, Liu Y, Zuo M, et al. Remodelling of cardiac sympathetic re-innervation with thoracic spinal cord stimulation improves left ventricular function in a porcine model of heart failure. *Europace*. 2015;17:1875–1883.

46. Olivas A, Gardner RT, Wang L, Ripplinger CM, Woodward WR, Habecker BA. Myocardial infarction causes transient cholinergic transdifferentiation of cardiac sympathetic nerves via gp130. *J Neurosci*. 2016;36:479–488.

47. Ballester M, Ferreira A, Carreras F. The myocardial band. *Heart Fail Clin*. 2008;4:261–272.

48. Crick SJ, Anderson RH, Ho SY, Sheppard MN. Localisation and quantitation of autonomic innervation in the porcine heart II: endocardium, myocardium and epicardium. *J Anat*. 1999;195(pt 3):359–373.

KEY WORDS arrhythmia, autonomic nervous system, cardiac innervation, denervation, hyperinnervation, myocardial infarction, neural remodeling, nerve sprouting, reperfusion therapy

APPENDIX For an expanded Methods section as well as supplemental figures and references, please see the online version of this paper.